Journal of Environment & Biotechnology Research
VINANIE PUBLISHERS
www.vinanie.com/jebr

Zero-valent iron nanostructures: synthesis, characterization and application

Maha M. El-Shafei,[1] Ahmed Hamdy,[1,*] M. M. Hefny[2]

[1] Sanitary and Environmental Engineering Research Institute (SEI), Housing and Building National Research Center (HBRC), Egypt
[2] Chemistry Department, Faculty of Science, Cairo University, Giza, Egypt

ORIGINAL RESEARCH ARTICLE

ABSTRACT

In this study, nano-scale zero valent iron (nZVI) was synthesized in the ethanol medium by reduction of ferric iron using sodium borohydride as a reducing agent under atmospheric conditions. The synthesized iron nanoparticles are mainly in zero valent oxidation state and remain without significant oxidation for weeks. A methodical characterization of nZVI was carried out using XRD, SEM, TEM, UV and FTIR studies. The acquired iron nanoparticles consist of a zero valent core embracing a rest oxide shell. The iron nanoparticles diameter was predominantly in the range of 10-100 nm. The laboratory synthesized nZVI particles was examined for methylene blue (MB) removal efficiency from aqueous solution in relation to the contact time, dye concentration and temperature. The increase in the contact time and temperature enhanced the dye decolorization. The degradation decreased from 91.7 to 72.0% on increasing the concentration of dye from 10 to 70 mg/L. These findings elucidated the rapid removal of MB by nZVI and the feature of the synthesized nZVI particles to treat MB contaminated wastewater.

KEYWORDS
Characterization; Methylene blue; Nano-scale zero valent iron; Removal efficiency; Synthesis

1. INTRODUCTION

Nanotechnology is a new scientific field being developed since 1980s. It is the doctrinaire of individual molecules and atoms to create devices and materials with inherent properties. The physical and chemical properties of metal nanoparticles are fundamentally determined by its shape, structure, crystallinity, size and structure (Madhavi et al., 2013). In recent years, nZVI has attracted attention of researchers. In particular, nZVI has been used in the treatment of nitrate contaminated solution due to its unique atomic properties, abundance, high reduction capacity, high efficiency, magnetic property, molecular and chemical properties (Zazouli et al., 2014), (Harman and Genisoglu, 2016). Also, the mobility, toxicological impact, long-term fate and environmental stability of nZVI have received increasing attention. nZVI and its derivatives including surfactant-stabilized nZVI and bimetallic nZVI were employed in more than 50 pilot scale or full-scale remediation sites in various countries for remediation of underground soil and water (Han et al., 2015), (Dutta et al., 2016).

The application of nZVI in treatment of wastewaters comprises of various metallic ions such as Cr^{3+}, Cu^{2+}, Ba^{2+}, Pb^{2+}, etc. has proven to be successful (Prabu et al., 2015), (Allabaksh et al., 2010). In addition, nZVI has been used as an effective filling material for permeable reactive barriers (PRBs), (Fakhri and Adami, 2013), and are well recognized as an prominent technology for the in situ degradation of a vast range of pollutants due to their benign properties and high reactivity (He et al., 2016). nZVI can be used in water systems and transported effectively by water flow owing to its smaller particle size and higher surface area to volume ratio than bulk ZVI (Wang et al., 2009; Watts et al., 2015). Generally, nZVI offers several advantages

Corresponding author: **Ahmed Hamdy**
Tel: +201228674325
Fax: +20233351564
E. mail: a.hamdy2@aol.com

Received: 09-11-2017
Revised: 01-12-2017
Accepted: 16-12-2017
Available online: 01-01-2018

including (1) a raise in the reaction rate of reductive degradation; (2) minimize dose of reduction material; (3) control over the risk of toxic intermediates releases; and (4) a nontoxic end product generation (Hwang et al., 2011). nZVI technology is becoming a public choice for treatment of toxic and hazardous wastes, as the miniature size of the iron nanoparticles helps to foster effective subsurface dispersal whilst their large specific surface area match to reinforce reactivity for fast transformation of contaminant. Recent inventions in production and nanoparticle synthesis have resulted in increased availability of zero-valent iron nanoparticles (nZVI) and fundamental cost reductions for large scale applications (Namasivayam and Raju, 2013).

Various synthetic methods have been developed for nZVI production, such as ball-milling and iron oxides thermal reduction (Panturu et al., 2010). In many scenarios of real field remediation, nZVI particles were stabilized by encapsulation with carbon matrices or silica or surfactants (Zhang, 2003), (Han et al., 2015). The method most widely used for environmental purposes is the borohydride reduction of Fe (III) or Fe (II) ions in aqueous media. The major advantage of this chemical reduction method are its chemical uniformity and simplicity (Hwang et al., 2011). The production of metal nanoparticles via reductive precipitation consists of three steps: 1) homogeneous nucleation, 2) growth of particle nuclei, and 3) ripening or agglomeration (Han et al., 2015). In the above studies, the nZVI synthesis was performed in inert conditions to keep iron in its zero valent form. However, the synthesized nZVI tends to form oxides/ hydroxides such as Fe_2O_3, Fe_3O_4 and FeOOH and it is unstable in atmospheric conditions (Liu et al., 2014), (Zhang et al., 2015).

During the last years many research papers have been published on nZVI synthesis in aqueous medium. However, iron nanoparticles synthesis in ethanol medium has not been well documented. Hence, the thematic of this present investigation is to synthesize nZVI in open air in presence of ethanol to prohibit massive oxidation and to characterize the synthesized materials in terms of its surface properties and size (Yuvakkumar et al., 2011).

Methylene blue (MB) is chemical compound from heterocyclic aromatic compounds have the molecular formula $C_{16}H_{18}N_3SCl$. It is most considerably used as a substance for dyeing silk, wood and cotton and has number of biological uses. It has severe impact on human health; for example ingestion through the mouth may cause nausea, vomiting, diarrhea, etc. Thus, removal of MB from wastewater is of considerable interest from an environmental point of view (Arabi and Sohrabi, 2014). In this study we have synthesized and characterized the iron based nano scale particles and zero oxidation state. The materials characterization was performed using X-Ray diffraction instrument (XRD) to determine the crystal structures of nZVI particles, transmission electron microscopy (TEM), scanning electron microscopy (SEM) equipped with energy-dispersive X-ray spectroscopy (EDX), ultraviolet–visible spectroscopy (UV-VIS), and Fourier-transform infrared spectroscopy (FT-IR).

2. MATERIALS AND METHODS

2.1. Materials

Ferric chloride ($FeCl_3.6H_2O$) and Sodium borohydride ($NaBH_4$) were purchased from Loba Chemie, India and Winlab Co., UK respectively. MB was obtained from (Farbwerke Hoechst AG; BP 58 Germany) and was used without further refinement. All other reagents were analytical reagent grade. Deionized water was used throughout this study.

2.2. Preparation of nZVI particles

The synthesis of nZVI was carried out through reduction of Fe(III) using borohydride (Wang et al., 2006). For this purpose, sodium borohydride ($NaBH_4$) and iron (III) chloride hexahydrate ($FeCl_3.6H_2O$) were used. In each batch of synthesis, 1 g of $FeCl_3.6H_2O$ was dissolved in a 4/1 (v/v) ethanol/water mix (75 mL ethanol + 25 mL deionized water) and stirred on a magnetic stirrer. About 0.33 M sodium borohydride solution was prepared. The borohydride solution was poured in a burette, and then added dropwise to the Fe (III) solution by stirring of the mixture on a magnetic stirrer. A black precipitate immediately appeared after the first drop of sodium borohydride solution was added. After adding the whole borohydride solution, the mixture was left for further 15 min of stirring. The redox reaction can be represented by:

$$4Fe^{+3} + 3BH_4^- + 9H_2O \rightarrow 4Fe^0{}_{(s)} + 3H_2BO_{3\,(aq)}^- + 12H^+ + 6H_2 \qquad (1)$$

Iron nanoparticles were separated from the liquid phase by vacuum filtration, in which two sheets of Whatman filter papers of 0.45 μm were used in each filtration process. At this point, the solid particles were washed three times with 25 mL portions of absolute

ethanol to remove water. This washing process is probably the key step of synthesis since it prevents the rapid oxidation of zero-valent iron nanoparticles. The synthesized nanoparticles were finally dried in oven at 105°C till overnight (Li et al., 2015).

2.3. Adsorption experiments

The adsorption of MB onto nZVI was achieved using batch experiment method. The effect of contact time, MB initial concentration and temperature were investigated using protocol as follows; 50 mL of dye solution of known initial concentration (10–70 mg/L) was shaken with a certain amount of the adsorbent (0.5 g) on a horizontal shaker at 150 rpm at the default pH. The contact time was changed from 0 to 120 min. Sample solutions were withdrawn at predetermined time intervals to determine the extent of color removal. The influence of temperature on adsorption of the MB was investigated at 303, 313 and 323 K under the optimized conditions of contact time (120 min) and nZVI dosage (0.5 g). After each predetermined time interval, samples were withdrawn from the conical flasks and the MB solutions were separated from the adsorbent by filtration which is subsequently followed by centrifugation. The residual dye concentration in the supernatant solutions was tested using a spectrophotometer (T70+ UV/VIS Spectrometer, PG Instruments Ltd, UK) at a wavelength of 665 nm.

The percentage removal of MB by nZVI was determined using the formula (Geçgel et al., 2013):

$$R\,(\%) = \frac{C_i - C_f}{C_i} \times 100 \qquad (2)$$

where C_i and C_f are the initial and final MB concentration before and after adsorption (mg /L); R (%) is the MB removal efficiency (%).

The adsorption capacity of MB on nZVI was determined using the following equation (Malina and Rađenović, 2015):

$$q = \frac{(C_o - C_e) \times V}{W} \qquad (3)$$

Where C_o and C_e are the initial and given time MB concentrations (mg/L), respectively, q is the quantity of MB adsorbed per unit mass of nZVI (mg/g), V is the volume of MB solutions (L) and W is the weight of sorbent (g).

2.4. Characterization

2.4.1. X-Ray diffraction (XRD)

XRD analysis of Fe^o nanoparticles was performed using (X-Pert – PRO – PANalytical Netherland) at 45 kV and 30 mA. The instrument uses Cu Kα radiation and graphite monochromator to give X-rays with wavelength of 1.54 Å. Fe^o nanoparticles were placed in glass holder and scanned from 4° to 80°. Scanning step was 0.5 Sec. The peak at 2θ of 44.8096° indicates the existence of iron nanoparticles (Fe^o). Particle size can be presumed with the XRD by using Scherer equation (Fan et al., 2010):

$$D = \frac{0.9\lambda}{\beta \cos\theta} \qquad (4)$$

where D is the size of particle (nm), β is the full width at half maximum (FWHM), λ is the Cu Kα radiation wavelength, i.e., 0.154 nm, and θ is the Bragg angle obtained from 2θ corresponding to maximum peak intensity (Hwang et al., 2011), (Dutta et al., 2016).

2.4.2. Scanning electron microscopy (SEM)

SEM (FE-SEM, Quanta FEG 250, Philips, USA) equipped with energy-dispersive X-ray spectroscopy (EDX), was used to qualitatively determine the morphology, size and composition of the samples. The nZVI sample was dispersed on the agglutinant carbon tape which is propped on a metallic disk. Images of the ZVI nanoparticles surface were taken at different magnifications. Simultaneously, EDS spectrum was recorded at selected areas on the nZVI surface to give information about chemical composition and surface atomic distributions.

2.4.3 Transmission electron microscopy (TEM)

TEM (JEM-2100, HR-TEM, Japan) analysis was also performed to reveal the morphology of samples and particle size. The dried particles were dispersed in ethanol, dropped into the carbon net and vaporized to dryness.

2.4.4. Ultraviolet-visible spectroscopy (UV-Vis)

The UV–Vis spectrum of Fe^o nanoparticles was recorded using UV–Vis spectrophotometer, at the range of 190-600 nm.

2.4.5. FTIR spectra analysis

FT/IR-4100 type A spectrometer, JASCO, Japan was used to compare the samples. The sample and KBr were mixed with a ratio of 1:100 and flattened under high

pressure; afterwards they were immediately tested in the range 450–4000 cm^{-1} with a resolution of 4 cm^{-1}.

3. RESULTS AND DISCUSSION

3.1. Characterization of synthesized nZVI particles

The XRD analysis of Fe^0 nanoparticles is shown in (Figure 1). The peak at 2θ of 44.8096° which represent 100% intensity indicates the presence of α-Fe^0 nanoparticles in the sample. The peak at 2θ = 31.8197° indicate the existence of iron oxide (Fe_2O_3 or Fe_3O_4). The mean crystalline dimension of the Fe^0 nanoparticle was found to be 44.43 nm and lattice strain to be 0.0021 when calculated by Scherer equation. Similar results was observed in other studies (Taha and Ibrahim, 2014; Fan et al., 2009). Figure 2a shows the SEM images of the synthesized nZVI. The iron particles appear spherical and have a size distribution within 20–100 nm, demonstrating the characteristic chain-like morphology. Aggregation of the iron nanoparticles is reported to be caused by the magnetic dipole–dipole interactions and large surface area of the individual particles. Similar results were observed in other studies (Taha and Ibrahim, 2014; Üzüm et al., 2008). Literature resources indicate that nZVI possess a core–shell structure, in which the shell represents the oxidized part that surrounds the Fe core and preserves it against further oxidation. At selected area (Figure 2b) EDS spectrum shows strong signal in the iron region and confirms the formation of nZVI as shown in (Figure 2c). The nZVI internal structure was determined by transmission electron microscope (TEM) (Figure 3). The spheres having diameters of around 10-100 nm can be distinguished from each other and matches with SEM results which show the existence of the core and the shell layer of the nZVI particle. The dusky color acts as the core whilst the lighter color acts as the nZVI shell. These results are generally consistent with other studies (Han et al., 2015), (Yuvakkumar et al., 2011) and (Jamei et al., 2013)proposes a core–shell structure for nZVI. Normally, nanoparticles scatter visible light rather than absorption and wavelength (λ_{max}) increases with the decrease in particle size. UV-Vis can be used to determine certain compounds utilized in the functionalization of nanoparticles for dispersions and applications. Changes in the UV region of the spectrum can be usually contributed to charge transfer (CT) bands between the functional ligand and surface metal cation (Madhavi et al., 2013). From UV-Vis spectrum of nZVI particles (Figure 4), it was observed that a smooth and narrow absorption bands were obtained at 196.8 nm, 199.8 nm, 205 nm and 368.3 nm corresponding to the excitation of surface plasmon vibrations in the nZVI solution which is characteristic of monodispersed iron nanoparticles. Different results was reported by many studies (Allabaksh et al., 2010)(Pattanayak et al., 2013) (Yuvakkumar et al., 2011).

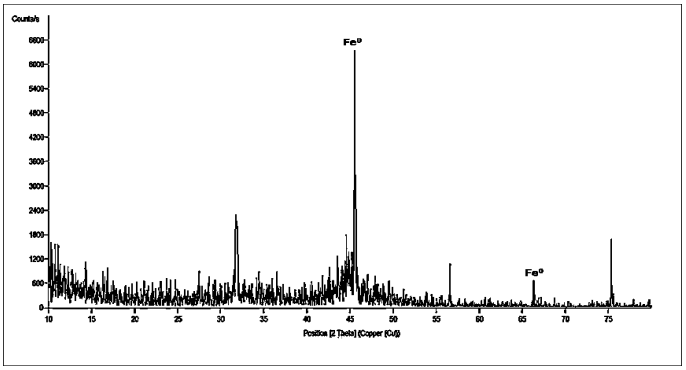

Figure 1. X-ray diffraction (XRD) pattern of nZVI particles.

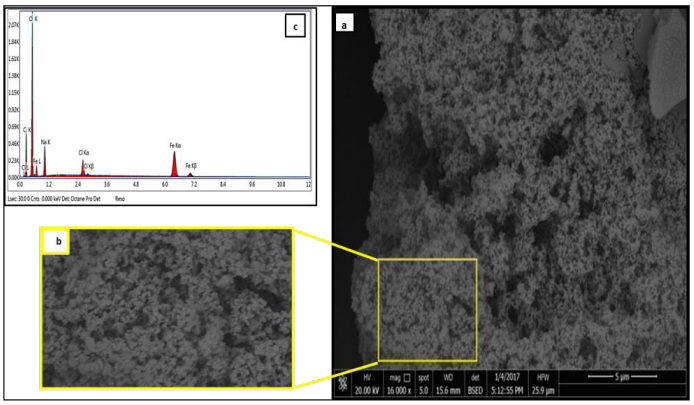

Figure 2. SEM image of nZVI particles (a), SEM selected area image of nZVI (b), EDS spectrum of nZVI particles (c).

As displayed in (Figure 5), the FTIR spectrum of synthesized nZVI showed peaks at 3421, 1638, 1415, 1359, 1042 and 610 cm^{-1}. The band at 3421 cm^{-1} corresponds to weak stretching vibration of surface hydroxyl groups. The peak at 1638 cm^{-1} was due to attraction of some water molecules on the surface of the nZVI in the form of physical adsorption, the bands at 1415 and 1359 cm^{-1} can be assigned to the asymmetric stretching vibration of –COO- functional groups. The bands at 1042 cm^{-1} and 610 cm^{-1} correspond to iron, iron oxide nanoparticles respectively (Gao et al., 2016) (Madhavi et al., 2013).

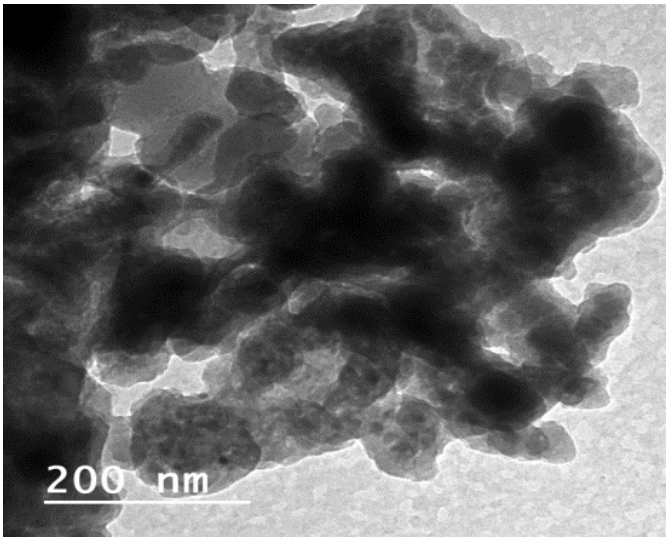

Figure 3. TEM image of nZVI particles

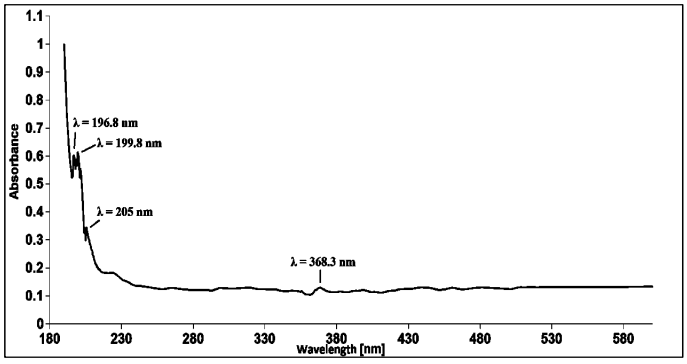

Figure 4. UV–Vis spectrum of nZVI particles.

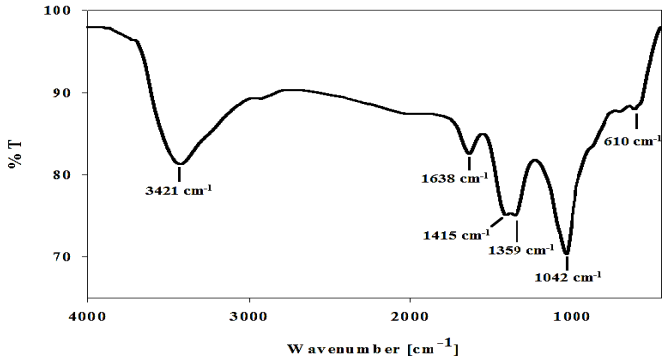

Figure 5. FTIR spectra of nZVI particles.

3.2. Adsorption

3.2.1. Effect of contact time and MB initial concentration

The influence of contact time on MB adsorption was studied by varying initial MB concentrations from 10 to 70 mg/L by fixing nZVI dosage at 0.5 g / 50 mL without pH adjustment. As shown in Figure 6a, the uptake of MB increased instantly and reached maximum within 30 min. The recorded uptakes were 0.7334, 0.7817, 0.8802 and 1 mg/g for MB initial concentrations of 70, 50, 30 and 10 mg/L, respectively. This was due to the presence of a large number of vacant adsorption sites on the surface of nZVI particles at the beginning of the process. Then, the amount of adsorbed MB did not significantly change with time due to the equilibrium of the repulsive forces between the MB molecules on the nZVI surface and in the bulk phases. This observation confirmed that the nZVI surface was saturated with the adsorbate at this point. It was evident from the Figure 6a that an increase in the initial concentration leads to decrease in absorption efficiency. This was because the increase in initial MB concentration resulted in saturation of the adsorption sites on nZVI surface. Therefore, MB adsorption increased very fast at initial stages due to rapid attachment of MB to the nZVI surface, followed by slow equilibrium attainment.

3.2.2. Effect of temperature

The effect of temperature on MB adsorption onto nZVI was investigated by varying temperatures (303, 313 and 323 K) at fixed nZVI dosage (0.5 g) and optimum pH. Figure 6b shows that an increase in the temperature from 303 to 323 K caused an increase in the adsorption capacity, indicating the endothermic nature of the adsorption process. The increase in temperature overcomes the activation energy barrier to increase the adsorption rate. The enhancement in the adsorption capacity could be correlated to the chemical interaction between MB and nZVI as well as creation of new adsorption sites or the increased rate of intraparticle diffusion of MB molecules into nZVI at higher temperatures (Arabi and Sohrabi, 2014). The MB removal efficiency of nZVI was determined to be 91.66, 99.51 and 100 % at 303, 313 and 323 K, respectively. The UV- Vis spectrum of MB before and after adsorption of MB by nZVI, revealed a difference in the intensity of the absorption peaks of the MB spectrum before and after treatment at each temperature (Figure 7). In addition, some absorption peaks of the MB spectrum disappeared and the intensity of some of them decreased, which confirmed the removal of MB by nZVI.

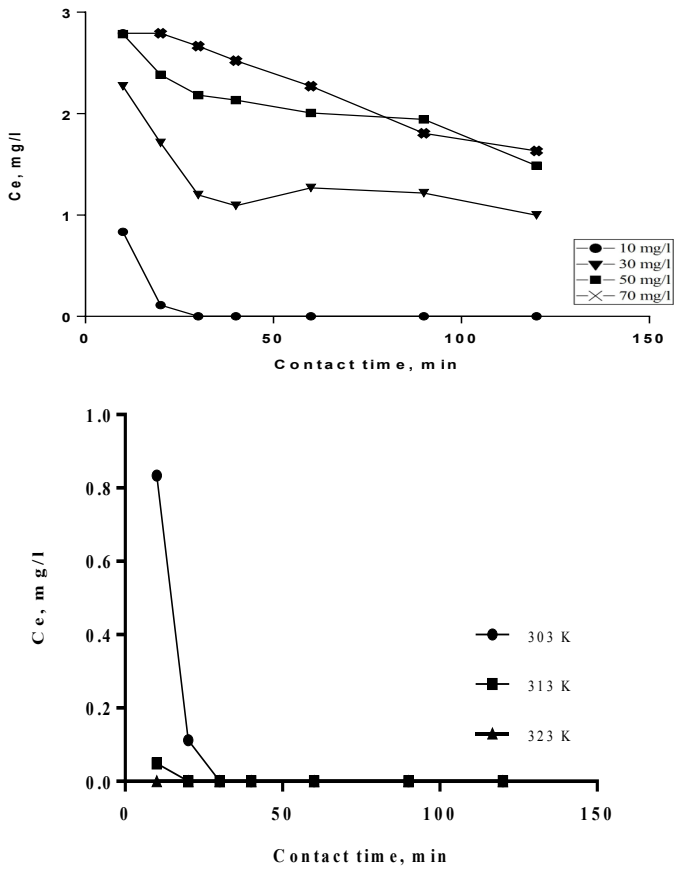

Figure 6. Effect of contact time and MB initial concentration (top image), effect of temperature on MB adsorption onto nZVI particles (bottom image).

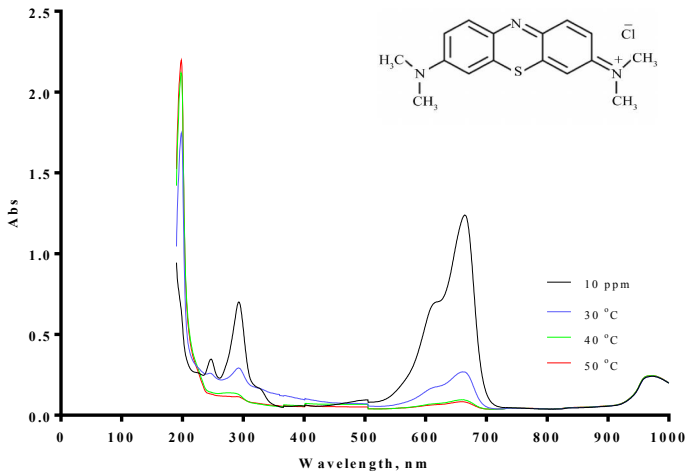

Figure 7. UV-Vis spectrum of MB before and after treatment at each temperature.

3.3. Kinetic studies

The pseudo-first-order kinetic model can be presented as (Gouamid et al., 2013):

$$\log(q_e - q_t) = \log q_e - \frac{k_1}{2.303}t \qquad (5)$$

where q_e and q_t are the amounts of MB (mg/g) at equilibrium and at time t, respectively, and k_1 is the pseudo-first-order adsorption rate constant (min^{-1}). A plot of log (q_e–q_t) vs t (Figure 8a) gives a straight line confirming the possibility of the applicability of the pseudo-first-order rate equation with a correlation coefficient (R^2 = 0.8374). From the plot, q_e and k_1 are specified from the slope and intercept respectively as presented in Table 1.

The pseudo-second-order adsorption rate equation may be expressed as follows (Hashemian et al., 2013):

$$\frac{t}{q_t} = \frac{1}{k_2 q_e^2} + \frac{t}{q_e} \qquad (6)$$

where k_2 (g/mg.min) is the rate constant of second-order adsorption. If second-order kinetics is viable, the plot of t /q_t versus t ought to show a linear relationship (Figure 8b). The q_e and k_2 values can be specified from the slope and intercept of the plot as presented in Table 1. The higher correlation coefficient (R^2 = 0.9983) indicates that the experimental data is best fitted into the pseudo second-order and suggests that the process of adsorption follows the pseudo-second-order kinetics which means the heterogeneity of the surface.

Table 1. The values of parameters and correlation coefficients of kinetic models for MB adsorption onto nZVI

Pseudo-first-order kinetic model				**Pseudo-second-order kinetic model**		
k_1 (min^{-1})	R^2	q_e (mg/g)		k_2 (g/mg.min)	R^2	q_e (mg/g)
0.012	0.837	0.116		0.394	0.998	0.855

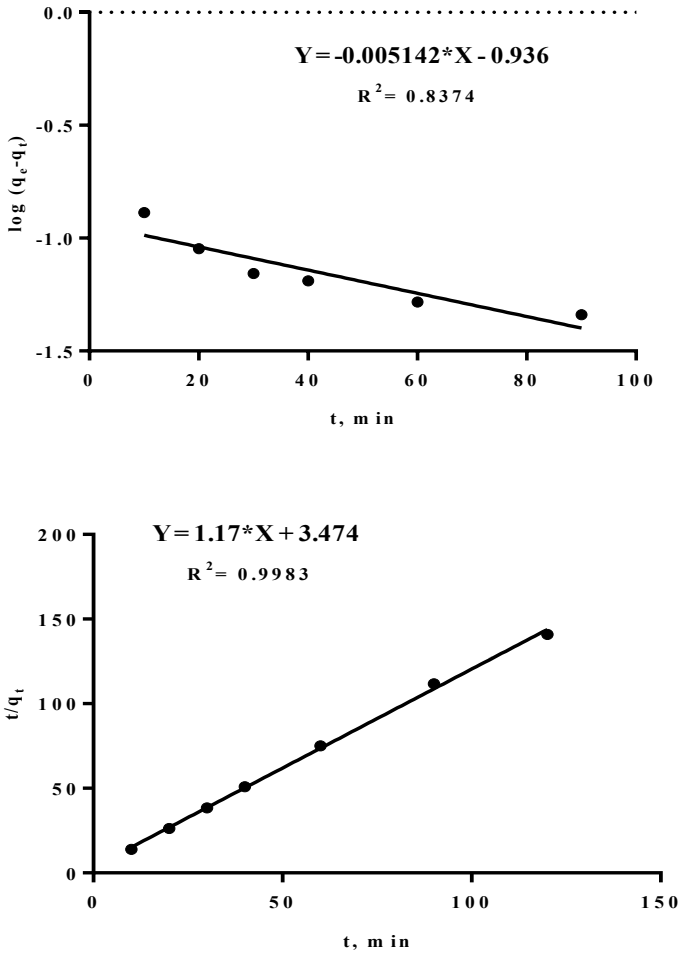

Figure 8. The pseudo-first-order kinetics (top image), the pseudo-second-order kinetics (bottom image) model polts for MB adsorption on nZVI at 30 °C.

3.4. Thermodynamic Studies

The spontaneity of adsorption process can be specified by thermodynamic parameters such as changes in enthalpy (ΔH°), free energy (ΔG°), and entropy (ΔS°). A spontaneous process will show a decrease in ΔG with an increase in temperature. The thermodynamic parameters of ΔG° (kJ/mol), ΔH° (kJ/mol), and ΔS° (J/mol.K) were determined by the following relationships (Gunasekar and Ponnusami, 2012):

$$\Delta G^o = \Delta H^\circ - T\,\Delta S^\circ \quad (7)$$

$$\Delta G^o = -RT\,\ln K^o \quad (8)$$

$$K^o = \frac{q_e}{c_e} \quad (9)$$

$$\ln K^o = \frac{-\Delta H^o}{RT} + \frac{\Delta S^o}{R} \quad (10)$$

where K° is the equilibrium constant, qe is the MB uptake (mg/g), C_e is the concentrations of MB (mg/L) at a given time t, T is the absolute temperature (K), and R is the gas constant (J/mol.K), ΔH° and ΔS° were determined from the slope and intercept of plot lnK° versus 1/T. Figure 9a shows the Van't Hoff plot for the adsorption of MB onto nZVI particles. The observed thermodynamic values are presented in Table 2. The negative value of ΔG° at all temperatures indicates the spontaneous nature and thermodynamically favorable of MB adsorption onto nZVI particles (Wei et al., 2016). The negative ΔG° values indicate that solutes tend to remain in the stationary phase rather than in the mobile phase (El-Latif et al., 2010), (Bocian et al., 2015), (El-Wakil et al., 2015). The positive value of ΔS° indicates the increased randomness at the solid–solution interfaces during adsorption and confirmed the high preference of MB adsorption onto nZVI particles. The positive value of the change in enthalpy indicates the endothermic nature of adsorption (El-Wakil et al., 2015), (Gunasekar and Ponnusami, 2012).

Table 2. Thermodynamic parameters for the adsorption of MB on nZVI particles ([MB] = 10 mg/L; nZVI dosage = 0.5 g/L)

T (K)	ΔG° (kJ/mol)	ΔH° (kJ/mol)	ΔS° (J/mol.K)	R²
303	-0.238	268.9	886.3	0.9879
313	-7.836	-	-	-
323	-18.549	-	-	-

The pseudo-second-order model was identified as the best kinetic model for MB adsorption onto the surface of nZVI particle. Accordingly, the rate constant (k_2) of the pseudo-second-order model was relied to determine the activation energy of adsorption by the following Arrhenius equation (Chen et al., 2010):

$$\ln k_2 = \ln A - \frac{E_a}{RT} \quad (11)$$

where k_2 (g/mg.min) is the rate constant for the pseudo second- order adsorption kinetics, A (g/mg.min) is the temperature-independent Arrhenius factor, E_a (kJ/mol) is the adsorption activation energy, R (8.314 J/mol.K) is the gas constant, and the T (K) is the absolute temperature. The activation energy (E_a) was obtained

from the slope of the plot of lnk_2 versus 1/T. Figure 9b shows the effect of temperature on the MB adsorption on nZVI particles (Arrhenius equation) and was 277 kJ/mol (R^2 = 0.9917) at 303 K for MB adsorption onto the nZVI particle surface and Arrhenius factor was 1.192 x 10^{48} (g/mg.min). The observed Arrhenius equation values are presented in Table 3.

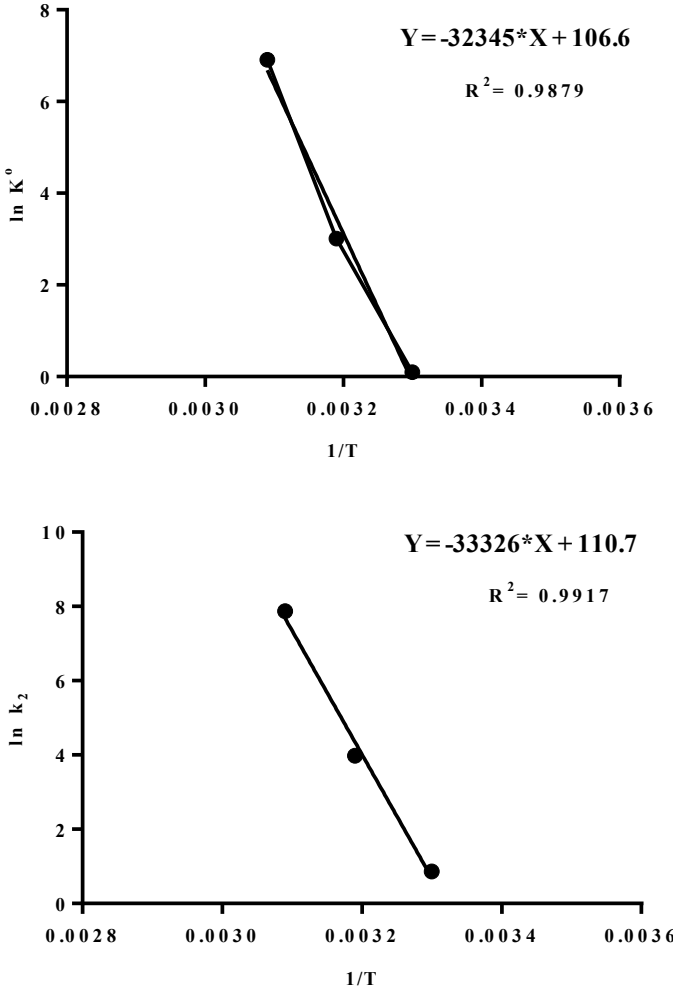

Figure 9. Van't Hoff plot (top image) and Arrhenius plot (bottom image) for the adsorption of MB onto nZVI particles.

Table 3. Arrhenius equation parameters for the MB adsorption onto nZVI particles.

Arrhenius equation parameters		
A (g/mg.min)	**R^2**	**E_a (kJ/mol)**
1.192x10^{48}	0.9917	277

The magnitude of the activation energy gives information on the physical or chemical nature of adsorption. Generally physisorption has energies in the range of 5–40 kJ/mol; higher activation energies (40–800 kJ/mol) propose chemisorption (Boparai et al., 2011). In this study, the activation energy value was higher than 40 kJ/mol (Table 3) indicating chemically controlled process as well as diffusion is not a limiting factor controlling the adsorption rate. Consequently, MB adsorption onto nZVI appears to occur by chemisorption spontaneous and endothermic adsorption has also been reported for the system of basic dyes on tree fern, wheat shell, mansonia wood sawdust, and hydrolyzed oak sawdust composite (El-Latif et al., 2010).

4. CONCLUSIONS

Nanoscaled zero valent iron (nZVI) (10-100 nm) was synthesized in the ethanolic medium by borohydride reduction method under atmospheric conditions. Synthesized nZVI characterization was carried out using XRD, SEM, TEM, UV and FTIR techniques. The results revealed that nZVI exists mainly in the zero oxidation state with 100% intensity at 2θ of 44.8096 º, have mean crystalline size of 44.43 nm and there was no significant oxidation observed during storage for weeks under atmospheric conditions through visual observation. SEM results revealed that nZVI appear as a spherical particle and tend to take shape of chain-like structures with a particle size in the range 20-100 nm and that nZVI have a strong trend to agglomerate in microscale aggregates due to the weak surface charges. TEM results revealed that nZVI exists abundantly in the form of zero-valent core surrounds by an oxide shell which preserves it against further oxidation and have diameters of around 10-100 nm can be distinguished from each other and this results are matched with SEM results. UV-VIS spectrum showed that four absorption peaks for nZVI which corresponding to wavelengths at 196.8 nm, 199.8 nm, 205 nm and 368.3 nm. FT-IR spectrum also showed six absorption peaks for nZVI at wavenumbers of 3421, 1638, 1415, 1359, 1042 and 610 cm^{-1}. Synthesized nZVI particles were successfully used as an adsorbent for MB removal from aqueous solutions. The results indicated that removal percentage was found to be 91.6% after 10 min for MB initial concentration of 10 mg/L. Kinetic results indicated that adsorption process followed the pseudo-second-order kinetic model with correlation coefficient (R^2 = 0.9983). This indicates that the adsorption rate was highly dependent on the availability of adsorption sites on nZVI surface rather than on MB concentration in the solution. A thermodynamic study was also

conducted and parameters indicated a spontaneous and endothermic process for adsorption of MB onto nZVI surface.

ACKNOWLEDGEMENTS

The authors gratefully acknowledge the Cairo University https://cu.edu.eg/ and Housing & Building National Research Center www.hbrc.edu.eg/ for providing facilities.

REFERENCES

Allabaksh, M.B., Mandal, B.K., Kesarla, M.K., Kumar, K.S., Reddy, P.S. (2010) Preparation of stable zero valent iron nanoparticles using different chelating agents. Journal of Chemical and Pharmaceutical Research, 2, 67-74.

Arabi, S., Sohrabi, M.R. (2014) Removal of methylene blue, a basic dye, from aqueous solutions using nano-zerovalent iron. Water Science and Technology, 70, 24-31.

Bocian, S., Soukup, J., Jandera, P., Buszewski, B. (2015) Thermodynamics study of solvent adsorption on octadecyl-modified silica. Chromatographia, 78, 21-30.

Boparai, H.K., Joseph, M., O'Carroll, D.M. (2011) Kinetics and thermodynamics of cadmium ion removal by adsorption onto nano zerovalent iron particles. Journal of Hazardous Materials, 186, 458-465.

Chen, M., Chen, Y., Diao, G. (2010) Adsorption kinetics and thermodynamics of methylene blue onto p-tert-butyl-calix [4, 6, 8] arene-bonded silica gel. Journal of Chemical & Engineering Data, 55, 5109-5116.

Dutta, S., Ghosh, A., Satpathi, S., Saha, R. (2016) Modified synthesis of nanoscale zero-valent iron and its ultrasound-assisted reactivity study on a reactive dye and textile industry effluents. Desalination and Water Treatment, 57, 19321-19332.

El-Latif, M.A., Ibrahim, A.M., El-Kady, M. (2010) Adsorption equilibrium, kinetics and thermodynamics of methylene blue from aqueous solutions using biopolymer oak sawdust composite. The Journal of American Science 6, 267-283.

El-Wakil, A., El-Maaty, A.W., Oudah, A.A.A.-R. (2015) Methylene blue dye removal from aqueous solution using several solid stationary phases prepared from *Papyrus* plant. Journal of Analytical & Bioanalytical Techniques, S13, 1.

Fakhri, A., Adami, S. (2013) Response surface methodology for adsorption of fluoride ion using nanoparticle of zero valent iron from aqueous solution. Journal of Chemical Engineering and Process Technology, 4, 161.

Fan, J., Guo, Y., Wang, J., Fan, M. (2009) Rapid decolorization of azo dye methyl orange in aqueous solution by nanoscale zerovalent iron particles. Journal of Hazardous Materials, 166, 904-910.

Fan, M., Yuan, P., Chen, T., He, H., Yuan, A., Chen, K., Zhu, J., Liu, D. (2010) Synthesis, characterization and size control of zerovalent iron nanoparticles anchored on montmorillonite. Chinese Science Bulletin, 55, 1092-1099.

Gao, J.-F., Li, H.-Y., Pan, K.-L., Si, C.-Y. (2016) Green synthesis of nanoscale zero-valent iron using a grape seed extract as a stabilizing agent and the application for quick decolorization of azo and anthraquinone dyes. RSC Advances, 6, 22526-22537.

Geçgel, Ü., Özcan, G., Gürpınar, G.Ç. (2013) Removal of methylene blue from aqueous solution by activated carbon prepared from pea shells (*Pisum sativum*). Journal of Chemistry, Article ID 614083, 9 pages

Gouamid, M., Ouahrani, M., Bensaci, M. (2013) Adsorption equilibrium, kinetics and thermodynamics of methylene blue from aqueous solutions using date palm leaves. Energy Procedia, 36, 898-907.

Gunasekar, V., Ponnusami, V. (2012) Kinetics, equilibrium, and thermodynamic studies on adsorption of methylene blue by carbonized plant leaf powder. Journal of chemistry, 2013.

Han, Y., Yang, M.D., Zhang, W., Yan, W. (2015) Optimizing synthesis conditions of nanoscale zero-valent iron (nZVI) through aqueous reactivity assessment. Frontiers of Environmental Science & Engineering, 9, 813-822.

Harman, B.I., Genisoglu, M. (2016) Synthesis and characterization of pumice-supported nZVI for removal of copper from waters. Advances in Materials Science and Engineering, Article ID 4372136, 10 pages.

Hashemian, S., Ardakani, M.K., Salehifar, H. (2013) Kinetics and thermodynamics of adsorption methylene blue onto tea waste/ $CuFe_2O_4$ composite. American Journal of Analytical Chemistry, 4, 1.

He, D., Ma, X., Jones, A.M., Ho, L., Waite, T.D. (2016) Mechanistic and kinetic insights into the ligand-promoted depassivation of bimetallic zero-valent iron nanoparticles. Environmental Science: Nano, 3, 737-744.

Hwang, Y.-H., Kim, D.-G., Shin, H.-S. (2011) Effects of synthesis conditions on the characteristics and reactivity of nano scale zero valent iron. Applied Catalysis B: Environmental, 105, 144-150.

Jamei, M.R., Khosravi, M.R., Anvaripour, B. (2013) Investigation of ultrasonic effect on synthesis of nano zero valent iron particles and comparison with conventional method. Asia-Pacific Journal of Chemical Engineering, 8, 767-774.

Li, X., Yang, Y., Gao, B., Zhang, M. (2015) Stimulation of peanut seedling development and growth by zero-valent iron nanoparticles at low concentrations. PloS One, 10, e0122884.

Liu, A., Liu, J., Pan, B., Zhang, W.-x. (2014) Formation of lepidocrocite (γ-FeOOH) from oxidation of nanoscale zero-valent iron (nZVI) in oxygenated water. RSC Advances, 4, 57377-57382.

Madhavi, V., Prasad, T., Madhavi, G. (2013) Synthesis and spectral characterization of iron based micro and nanoparticles. International Journal of Nanomaterials and Biostructures, 3, 31-34.

Malina, J., Rađenović, A. (2015) Kinetic aspects of methylene blue adsorption on blast furnace sludge. Chemical and Biochemical Engineering Quarterly, 28, 491-498.

Namasivayam, S.K.R., Raju, S. (2013) Synthesis, characterization and anti bacterial activity of chitosan stabilized nano zero valant iron. Bulletin of Pharmaceutical and Medical Sciences, 1, 7-11.

Panturu, R.-I., Jinescu, G., Panturu, E., Filcenco-Olteanu, A., Radulescu, R. (2010) Synthesis and characterization of zerovalent iron intended to be used for decontamination of radioactive water. UPB Scientific Bulletin, 72, 1454-2331.

Pattanayak, M., Mohapatra, D., Nayak, P. (2013) Green synthesis and characterization of zero valent iron nanoparticles from the leaf extract of Syzygium aromaticum clove. Middle-East Journal of Scientific Research, 18, 623-626.

Prabu, D., Parthiban, R., Kumar, P.S., Namasivayam, S.K.R. (2015) Synthesis, characterization and antibacterial activity of nano zero-valent iron impregnated cashew nut shell. International Journal of Pharmacy and Pharmaceutical Science, 7, 139-141.

Taha, M.R., Ibrahim, A. (2014) Characterization of nano zero-valent iron (nZVI) and its application in sono-Fenton process to remove COD in palm oil mill effluent. Journal of Environmental

Chemical Engineering, 2, 1-8.

Üzüm, Ç., Shahwan, T., Eroğlu, A.E., Lieberwirth, I., Scott, T.B., Hallam, K.R. (2008) Application of zero-valent iron nanoparticles for the removal of aqueous Co^{2+} ions under various experimental conditions. Chemical Engineering Journal, 144, 213-220.

Wang, Q., Snyder, S., Kim, J., Choi, H. (2009) Aqueous ethanol modified nanoscale zerovalent iron in bromate reduction: synthesis, characterization, and reactivity. Environmental Science and Technology, 43, 3292-3299.

Wang, W., Jin, Z.-h., Li, T.-l., Zhang, H., Gao, S. (2006) Preparation of spherical iron nanoclusters in ethanol–water solution for nitrate removal. Chemosphere, 65, 1396-1404.

Watts, M.P., Coker, V.S., Parry, S.A., Pattrick, R.A., Thomas, R.A., Kalin, R., Lloyd, J.R. (2015) Biogenic nano-magnetite and nano-zero valent iron treatment of alkaline Cr (VI) leachate and chromite ore processing residue. Applied Geochemistry, 54, 27-42.

Wei, W., Wang, Q., Li, A., Yang, J., Ma, F., Pi, S., Wu, D. (2016) Biosorption of Pb (II) from aqueous solution by extracellular polymeric substances extracted from *Klebsiella* sp. J1: Adsorption behavior and mechanism assessment. Scientific Reports, 6, Article number: 31575

Yuvakkumar, R., Elango, V., Rajendran, V., Kannan, N. (2011) Preparation and characterization of zero valent iron nanoparticles. Digest Journal of Nanomaterials and Biostructures, 6, 1771-1776.

Zazouli, M.A., Tilaki, R. A.D., Safarpour, M. (2014) Modeling nitrate removal by nano-scaled zero-valent iron using response surface methodology. Health Scope, 3, e15728.

Zhang, W.-x. (2003) Nanoscale iron particles for environmental remediation: an overview. Journal of Nanoparticle Research, 5, 323-332.

Zhang, Y., Chen, W., Dai, C., Zhou, C., Zhou, X. (2015) Structural evolution of nanoscale zero-valent iron (nZVI) in anoxic Co^{2+} solution: interactional performance and mechanism. Scientific Reports, 5, Article number: 13966.